Modeling trans-spinal direct current stimulation for the modulation of the lumbar spinal motor pathways

A Kuck[1], D F Stegeman[2] and E H F van Asseldonk[1]

[1] University of Twente, Drienerlolaan 5, 7522 NB Enschede, Netherlands
[2] Department of Neurology/Clinical Neurophysiology, Radboud University Medical Center, Donders Institute for Brain, Cognition and Behavior, Reinier Postlaan 4, 6500HB Nijmegen, Netherlands

E-mail: a.kuck@utwente.nl

Abstract

Objective. Trans-spinal direct current stimulation (tsDCS) is a potential new technique for the treatment of spinal cord injury (SCI). TsDCS aims to facilitate plastic changes in the neural pathways of the spinal cord with a positive effect on SCI recovery. To establish tsDCS as a possible treatment option for SCI, it is essential to gain a better understanding of its cause and effects. We seek to understand the acute effect of tsDCS, including the generated electric field (EF) and its polarization effect on the spinal circuits, to determine a cellular target. We further ask how these findings can be interpreted to explain published experimental results. *Approach.* We use a realistic full body finite element volume conductor model to calculate the EF of a 2.5 mA direct current for three different electrode configurations. We apply the calculated electric field to realistic motoneuron models to investigate static changes in membrane resting potential. The results are combined with existing knowledge about the theoretical effect on a neuronal level and implemented into an existing lumbar spinal network model to simulate the resulting changes on a network level. *Main results.* Across electrode configurations, the maximum EF inside the spinal cord ranged from 0.47 V m^{-1} to 0.82 V m^{-1}. Axon terminal polarization was identified to be the dominant cellular target. Also, differences in electrode placement have a large influence on axon terminal polarization. Comparison between the simulated acute effects and the electrophysiological long-term changes observed in human tsDCS studies suggest an inverse relationship between the two. *Significance.* We provide methods and knowledge for better understanding the effects of tsDCS and serve as a basis for a more targeted and optimized application of tsDCS.

Keywords: tsDCS, computational modeling, neurorehabilitation, spinal cord injury

(Some figures may appear in colour only in the online journal)

1. Introduction

Spinal cord injury (SCI) poses a heavy burden on the quality of life. Depending on the severity and location of the injury, sufferers are usually left with the loss of upper and lower limb motor control, as well as other vital functions. Among other investigated treatment options, there is a recent focus on invasive and non-invasive electrical stimulation techniques with the intention of inducing an additional degree of improvement when combined with traditional rehabilitation efforts.

Stimulation protocols under investigation for SCI rehabilitation vary significantly in their degree of invasiveness and intended neural response. Whereas for non-invasive electrical stimulation, electrodes are placed on the skin of the subject (Cogiamanian *et al* 2012), invasive electrical stimulation of the spinal cord has been successfully demonstrated by using

epidural electrodes (Harkema *et al* 2011, Wenger *et al* 2016, Alam *et al* 2017).

In humans, both invasive and non-invasive electrical stimulation have been used to directly activate the targeted neural pathways in the spinal cord via supra-threshold electrical stimulation. Sub-threshold network modulation is commonly applied non-invasively and aims to modulate ongoing and future neural activity by inducing pathway specific plastic changes.

We focus here on the understanding of noninvasive sub-threshold direct current stimulation (DCS) for the modulation of the lumbar spinal motor circuits. Trans-spinal direct current stimulation (tsDCS) aims to modulate spinal motor pathways and in turn, increase and direct neural plasticity where it is most necessary (for a review see: Cogiamanian *et al* (2012)). A well understood and targeted application is essential for the success and credibility of the tsDCS technique in a rehabilitation setting. Therefore, next to existing practical efforts, a reasonable way of directing the effects of tsDCS has to be found. However, predictions of the short and long-term effects of DCS are difficult, since they require a thorough understanding of the functional and anatomical parameters of the nervous system.

Previous studies have shown, that tsDCS can have a significant effect on the pathways in the spinal cord including the descending motor pathways (Bocci *et al* 2014), ascending somatosensory pathways (Cogiamanian *et al* 2008) and the lumbar monosynaptic reflex loop (Lamy *et al* 2012, Hubli *et al* 2013). In the latter, modulatory effects on post activation depression (PAD) (Winkler *et al* 2010) and presynaptic inhibition (Yamaguchi *et al* 2013) have also been shown. Additionally, animal studies provide further evidence on effects of DC stimulation on the spinal circuits. Thereby, lumbar tsDCS had a wide range of influences on, for instance, the execution of descending motor signals, spontaneous firing measured in the motor nerve as well as associative plasticity when paired with trains of cortical signals (Ahmed 2011, 2013a, 2013b). All studies suggest a clear polarity dependency of the reported effects. The growing evidence raises hope that tsDCS may be applicable to the rehabilitation of SCI or even extend to other disorders in the future. For a successful application however, the distribution and magnitude of the applied electric field (EF), its acute effects on the targeted neural pathways and the relationship to the long term effects reported in literature have to be investigated.

DC stimulation generates a weak EF of <1 V m^{-1} for tsDCS (Parazzini *et al* 2014) as well as for the related transcranial DCS technique (tDCS) (Datta *et al* 2009, Salvador *et al* 2010, Rampersad *et al* 2014). The interaction with a neural structure thus leads to a local shift in transmembrane potential, depending on the detailed morphology and its alignment with the EF. Assuming a spatially static EF, membrane polarization takes place mainly at closed ends such as axon and dendrite terminals. The polarization exponentially decays with further distance to the terminal.

The molecular working mechanisms within the neuron are largely dependent on its resting membrane potential. Membrane polarization will therefore lead to an acute functional modulation of the neuron and can be measured as a change of synaptic efficacy (Rahman *et al* 2013). The ultimate goal is to translate such acute effects into long term changes via mechanisms known as synaptic plasticity. This transition depends on the acute membrane polarization and the molecular mechanisms involved (cellular targets), the duration of the stimulation (Bindman *et al* 1964, Gartside 1968, Rahman *et al* 2013), the ongoing neural activity (Fritsch *et al* 2010, Ranieri *et al* 2012) as well as subject specific genetics factors (Lamy and Boakye 2013).

Previous work shows that the polarization of a number of different cellular targets (e.g. soma, dendrites, axon terminals (ATs)) may be eligible to produce the observed plasticity effects in synaptic efficacy. Thereby facilitation/inhibition of neuron function may be causally related to depolarization/hyperpolarization of the somatic membrane potential (Jefferys 1981, Bikson *et al* 2004, Radman *et al* 2009, Rahman *et al* 2013). The polarization of incoming axons (Bikson *et al* 2004, Arlotti *et al* 2012, Kabakov *et al* 2012, Rahman *et al* 2013) and ATs (Hubbard and Willis 1962, 1968, Rahman *et al* 2013) may further contribute to the effects of DCS. In pyramidal neurons, typically the focus of cortical tDCS studies, the polarization of apical dendrites, which polarize opposite to somas, was also found to influence synaptic processing (Bikson *et al* 2004, 2013, Kabakov *et al* 2012).

The so far gathered knowledge underlines the importance of understanding the cellular targets of DCS as a prerequisite to a rational electrotherapy design (Bikson *et al* 2013). Most previous work aimed at the understanding of DCS on cortical structures. Our focus differs in this respect, since we focus on the application of DCS on the lumbar spinal motor circuits. This requires a thorough evaluation and analysis of spinal motoneuron (MN) morphology and functioning.

Alpha MNs receive axonal connections of cortical and local (sensory) origin. Dendrites extend radially around a central soma in a seemingly random fashion. For Ia terminals, a majority of synapses are located on the proximal dendrites and follow little distinct patterns of spatial organization (Burke and Glenn 1996, Burke 1968, Segev *et al* 1990, Rotterman *et al* 2014). Motoneuron response and excitability may be controlled via channels exhibiting persistent inward currents (PIC) (Heckman *et al* 2008), located on the proximal dendrites (Elbasiouny and Mushahwar 2007, Powers *et al* 2012).

Previous publications have shown that tsDCS can modulate spinal network output. The goal of our contribution is a thorough analysis of the EFs generated by tsDCS, as well as the resulting membrane polarization in neurons, sensory and descending corticospinal ATs. Concurrently, we seek to find the cellular target of tsDCS, including its theoretical effects on a network level. Along this line, we further aim to understand the connection between simulated, acute network effects and long term plasticity changes reported by others as well as the impact of possible electrode misplacements.

We use a realistic full body segmented finite element model to estimate the EF inside the spinal cord when stimulated with three different electrode configurations at an intensity of 2.5 mA. We apply the EF finite element solution to realistic neuron models to investigate changes in membrane resting potential within the neuron as well as afferent and efferent ATs. We

further combine the observed membrane polarization effects with acute cellular changes found experimentally by others. To simulate the theoretical network effect we make use of an existing lumbar spinal network model (Cisi and Kohn 2008).

2. Methods

2.1. Electrode placement

We simulated the EF for three electrode configurations (figure 1): (A) in previous publications used spine-shoulder configuration (active electrode on the T11 vertebrae and return electrode placed on the left posterior shoulder), (B) both electrodes placed at equal distance, superior and inferior to the T11 vertebrae, (C) the active electrode is placed on the T11 vertebrae and two counter electrodes are placed on the left and right anterior superior iliac crest.

2.2. Finite element model

The steady state electrical potential in the inhomogeneous volume conductor model is computed using the software environment SCIrun (Scientific Computing and Imaging Institute, Salt Lake City, UT, USA) by solving the function described by Poisson's equation

$$\nabla * (\sigma \nabla \Phi) = 0 \qquad (1)$$

where σ is a conductivity tensor and Φ is the electric potential. Subsequently the EF vector $\boldsymbol{E}$ is calculated by

$$\boldsymbol{E} = -\nabla \Phi. \qquad (2)$$

The goal is to solve equation (1), given a mesh, a set of known conductivities, and a set of known potentials corresponding to the electrode locations. Computations were conducted using a conjugate gradient descend algorithm at varying voxel resolutions of 4mm^3 in the head and extremities, 1–2 mm^3 in the torso and electrodes and 0.5mm^3 inside the spinal cord. The mesh was a pre-segmented full body model (Ella) (figure 2), which is part of the Virtual Population Library Version 2 (Christ *et al* 2010). A segmentation of the spinal cord into white and grey matter was added using a custom made model. Conductivities were adopted from Parazzini *et al* (2014) without change. White matter in the spinal cord was simulated using anisotropic conductivities with a transversal versus longitudinal factor of 1:10 (Miranda 2013). The rectangular surface electrodes (50 × 70 × 3 mm) were positioned according to the corresponding electrode configuration in direct connection with the skin surface. Electrode potentials were assigned to the outer surface nodes of each electrode mesh.

2.3. Motoneuron model

To calculate the influence of the steady state EF on motoneurons with a realistic morphology, six reconstructed cat motoneurons (NMO_00687, NMO_00688, NMO_00689, NMO_00690, NMO_00691, NMO_00692) initially supplied by Alvarez *et al* (1998) and modified by Balbi *et al* (2015)

were used (table 1). This was implemented via the modeling environment NEURON v.7.3 (Carnevale and Hines 2006). Each neuron model was placed in the ventral horn of the spinal cord between the T11 and T12 vertebrae (figure 3). Thereafter, the previously calculated extracellular potential for each compartment is calculated via trilinear-interpolation and assigned in NEURON via the extracellular function.

Two separate straight axons, representing efferent and afferent connections to the motoneuron, were assigned with the EF strength in longitudinal and anterio-posterior direction respectively at the level of the motoneuron. Both axons were modeled as simple cylinders with a length of 40mm and a diameter of 10 μm. Reported diameters for both axon types, including myelin, are within a range of 13 μm to 20 μm for afferent (Ia) fibers (Boron and Boulpaep 2012) and 16 μm to 20 μm for efferent axons originating from cortical Betz neurons (Hall and Guyton 2006, Patestas and Gartner 2006). The inner axonal diameter, without myelin, was estimated via multiplication of the g-ratio ($g = 0.6$) (Midroni and Bilbao 1995), whereby the chosen axon diameter of 10 μm is within the resulting range for both axons.

For all neural elements, the external resistivity was set to 70 $\Omega * $cm, the specific capacitance was set to 1 μF cm^{-2}. Na$^+$ and K$^+$ equilibrium potentials were set to +50 mV and −77 mV respectively, while the Ca^{2+} equilibrium potential dynamically changed depending on the variations of internal and external ion concentrations (Balbi *et al* 2015). For a complete overview of all biophysical parameters, which were adopted unchanged, refer to Balbi *et al* (2015).

2.4. Spinal circuit model

Simulations at a network level were performed using an open source lumbar spinal network model (ReMoto, Version: 2.1) developed by Cisi and Kohn (2008). The model employs two-compartment motoneuron models for slow (S), fast fatigue resistant (FR) and fast fatigable (FF) types and includes a population of interneurons (Ia reciprocal inhibitory interneurons, Ib interneurons, and Renshaw cells) connected to afferent connections and induced stochastic point processes associated with descending tracts. To simulate human electrophysiological experiments, the simulator incorporates external nerve stimulation with orthodromic and antidromic propagation. The generation of the H- reflex by the Ia-motoneuron pool system, its modulation by spinal cord interneurons, as well as varying possibilities for incorporating descending corticospinal motor-signals are included (Cisi and Kohn 2008).

2.5. Simulation procedure

As a first step, the local field potential distribution and EF for a stimulation intensity of 2.5 mA was computed for each electrode configuration (figure 1). To test the sensitivity of electrode misplacements, the active lumbar electrode was shifted vertically by ±5 centimeters. For configuration 'LSC ±' (figure 1(B)) the misplacement was applied to both electrodes.
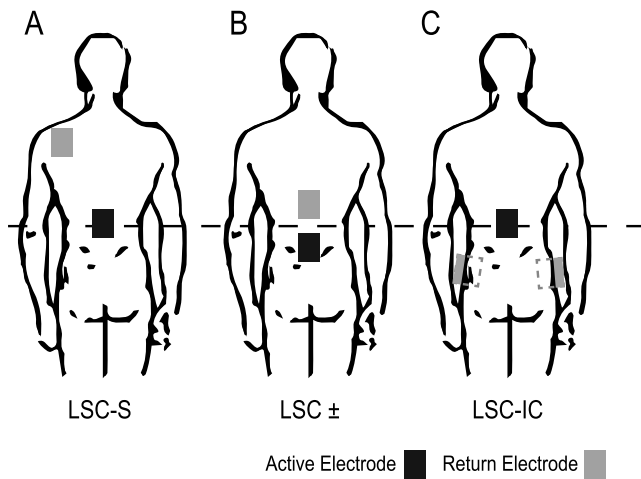
Figure 1. The simulated electrode placement configurations. (A) Active electrode on the lumbar spinal cord, return electrode on the posterior left shoulder. (B) Active electrode below and passive electrode above the lumbar spinal cord. (C) Active electrode on lumbar spinal cord, two passive electrodes on the left and right anterior superior Iliac Crest respectively.
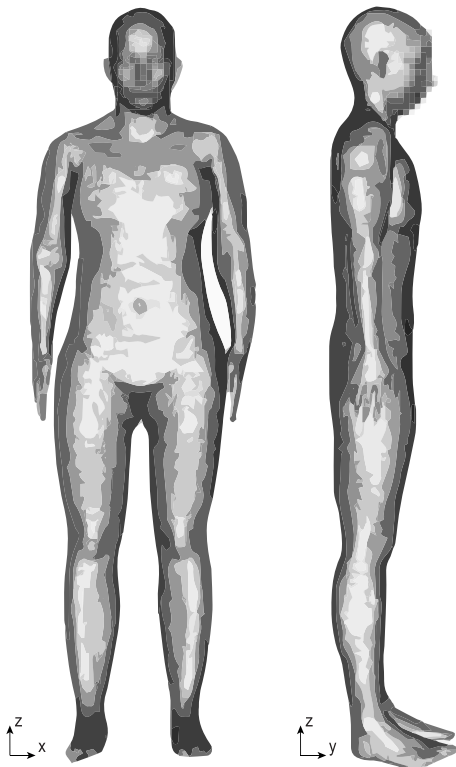

Figure 2. The utilized finite element model (Ella), which includes 22 individual segments, stems from the virtual population library (version 2) (dimensions: $500.4 \times 278.9 \times 1647.3$ mm).

Thereafter, each of the six neuron models was simulated at resting state with and without the applied EF for each of the three electrode configurations. The application of the EF results in a shift of the transmembrane potential.

To obtain results that can be related to experimental evidence, we used the spinal network model by Cisi *et al* (Cisi and Kohn 2008). The model is used to approximate the resulting acute functional changes imposed by tsDCS. We

therefore simulate two common functional tests used to assess (cortico-) spinal network function; these are the H- Reflex and motor evoked potentials (MEP). Both give information about spinal afferent and efferent motor pathways respectively and have been used to show effects induced by tsDCS in previous studies. We simulate the changes induced by modulation of the primary cellular target, including those during acute tsDCS, and compare the obtained network responses with experimental results obtained by others.

The neural building blocks used for both scenarios are: 800 slow (S), 50 fatigue resistant (FR) and 50 fast fatiguing (FF) motor units (Cisi and Kohn 2008). All other model parameters are left unaltered.

To mimic a spinal motoneuron response similar to that of a primary MEP, we simulate soleus voluntary contraction with a pulse input. Descending efferent input to the motoneuron pool is given by a single pulse Poisson distributed firing pattern, with a mean inter-spike-interval of 3 ms for $0\,\text{ms} \leqslant t \leqslant 5\,\text{ms}$ (Di Lazzaro *et al* 2003) and infinite otherwise (for details, refer to Cisi and Kohn (2008)). Baseline synaptic maximum conductance was set to 700 nS. Parameter values were chosen in favor of resulting in a clear model output, which is given by a simulated muscle activation in form of an EMG response. For each of the acquired EMG traces, the amplitude and delay are subsequently extracted.

For H-Reflex simulation, the afferent input is a single stimulus of 1 ms duration applied to the motor nerve for increasing stimulation amplitudes (H-Reflex).

3. Results

3.1. EF distribution in spinal cord

Figure 4 shows the calculated EF magnitude for all configurations throughout the spinal cord. Each configuration creates a distinct pattern with a maximum EF magnitude approximately half way between, and a smaller EF immediately adjacent to the two electrodes. The maximum field strength varies between $0.47\,\text{V m}^{-1}$ and $0.82\,\text{V m}^{-1}$ depending on the electrode placement.

A more thorough analysis of EF size and direction can be performed by regarding its individual vector components (figure 5). This is helpful when considering the directional prerequisite for the modulation of neural compartments.

For each electrode configuration the figure shows the transverse mean of the EF vector in all three dimensions. Thereby, the targeted motoneuron location is indicated by a red cross. Additionally the figure shows the EF for both, upward and downward (± 5 cm) misplacements respectively. For all configurations the transversal EF component remains small compared to anterio-posterior and longitudinal vector magnitudes. Also, though the anterio-posterior vector is largest below, the longitudinal component dominates between the electrode pair. Furthermore, a cyclic variation is visible on all vector components (see also figure 4). These appear to correlate with vertebral locations, and may therefore reflect a variation in EF magnitude caused by vertebral body anatomy.

Table 1. Morphometric parameters of the utilized motoneuron models.

|	NeuroMorpho identification number	Number of dendritic sections	Number of dendritic compartments	Number of primary dendrites	Soma diameter (μm)	Sum of diameters of primary dendrites	Soma surface (μm^2)	Surface of dendrites tree (μm^2)	Dendrites mean terminal distance
1	NMO_00687	398	3118	10	65.02	111.42	13 280	682 012	1049.45
2	NMO_00688	92	716	8	49.97	87.38	7847	150 243	736.52
3	NMO_00689	86	540	16	65.64	158.97	13 535	166 343	456.83
4	NMO_00690	149	1425	13	52.82	89.10	8767	233 642	829.38
5	NMO_00691	249	2183	11	60.81	101.77	11 616	374 199	896.49
6	NMO_00692	270	2656	12	63.83	130.10	12 801	489 120	891.33
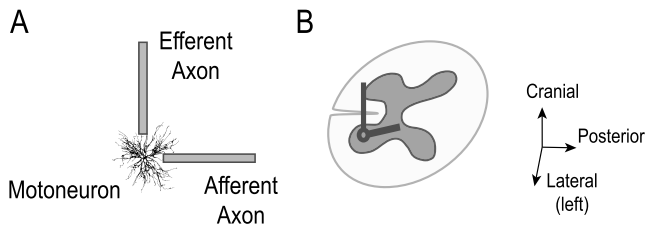
Figure 3. (A) Schematic illustration of the utilized motoneuron model, essentially consisting of three separate models: a realistic neuron model and two straight, cylindrical axons. (B) The location and orientation of motoneuron and axon models within the spinal cord (axon length not to scale). The motoneuron is placed within the grey matter below the T11 vertebrae.

When the active electrode is misplaced, EF amplitude and direction at the stimulation target site are altered. For cases where the active electrode is placed on top of the target region, misplacements lead to amplitude changes in anterio-posterior and field reversals in longitudinal direction (figures 5(A) and (C)). When two electrodes are placed in equal distance to the target region, a misplacement of both affects the field magnitude in longitudinal and lead to a reversal in anterio-posterior direction (figure 5(B)).

3.2. Changes in membrane potential

The potential distribution at motoneuron level and the resulting membrane polarization for an exemplary motoneuron is shown in figure 6. Clearly visible is the de-/hyperpolarization trend in line with the EF-vector direction. In this case, as for all tested motoneuron/configuration pairs, afferent and efferent axon terminal polarization (ranging from 0.24 mV to 1.41 mV) was dominant and multiple times stronger compared to other cellular targets (figure 7). In contrast, the soma was hardly polarized (<0.004 mV) and polarization of dendritic terminals did not exceed 0.15 mV. From further analysis it follows that the mean polarization of dendritic membrane, specific to PIC channels and synaptic terminal locations (<0.037 mV), was approximately three times lower than the dendritic maximum (figure 7).

For electrode misplacements, efferent axon terminal polarization may increase or reverse depending on the shift direction (figures 7(A) and (C), col. 4) when the active electrode is placed on the target region. Afferent terminal polarization is affected little in this case, whereby amplitude is altered by preserving effect direction. For equal distance placements, misplacement may change sign and amplitude of afferent
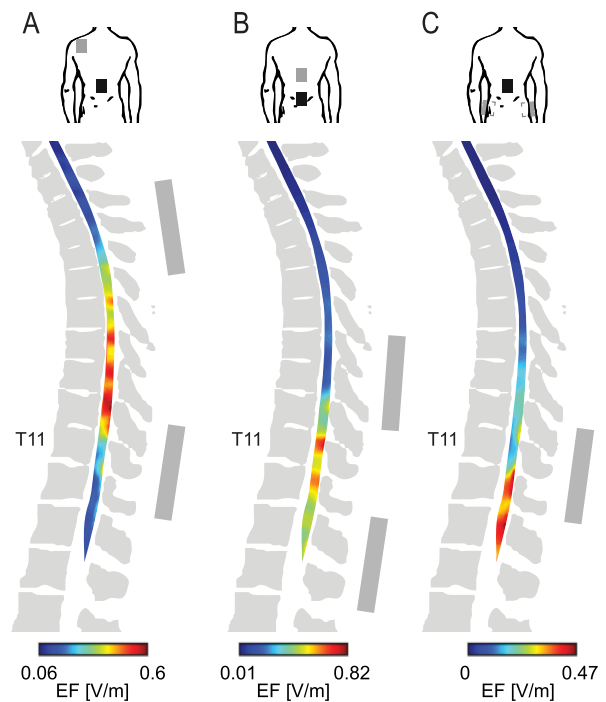

Figure 4. EF distribution in the spinal cord for each electrode configuration with indicated electrode locations (see also figure 1).

axon's terminal polarization (figure 7(B) col. 5). Efferent axon terminal polarization amplitude is modulated while preserving effect direction.

3.3. Spinal network simulation

In the previous subsections, we showed the acute polarization effects on lumbar spinal structures and identified the most dominant cellular target. Subsequently, we use the spinal network model developed by Cisi and Kohn, to perform a sensitivity analysis by modulating the identified cellular target to understand the resulting effects on a network level. We limit the analysis to effects caused by axon terminal polarization, representing the most prominent cellular target as shown above (figure 7). Acute, (post)synaptic effects of axon terminal polarization are known from literature (Rahman *et al* 2013), reporting an EF dependent change in EPSP amplitude.

The equation that expresses synaptic connections via the postsynaptic current I_{syn} can be written as:
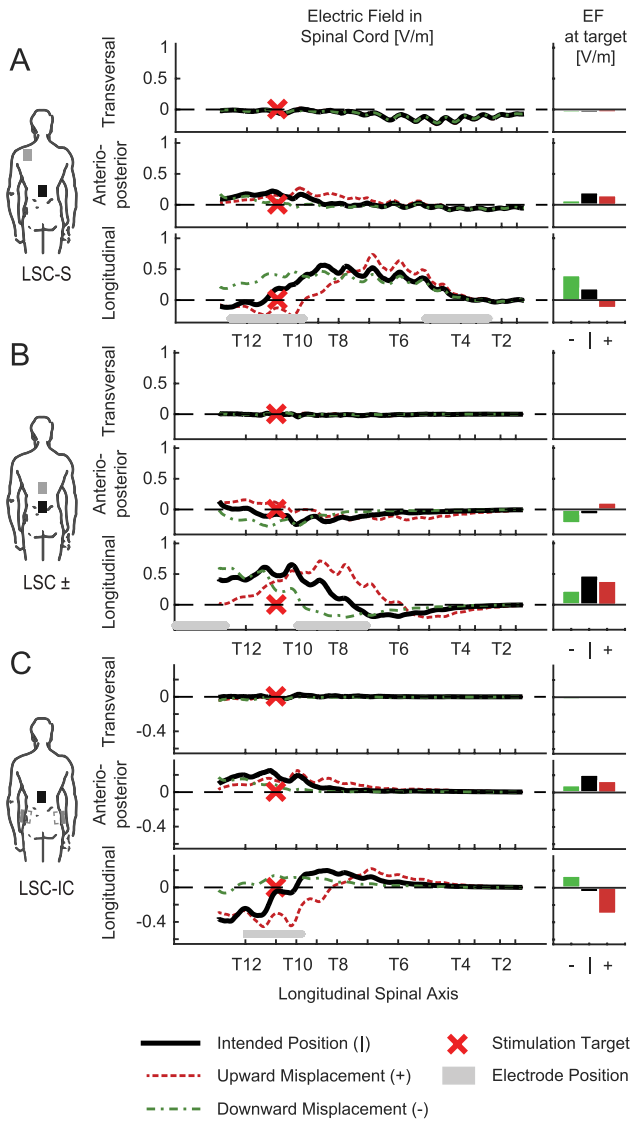
Figure 6. Stimulus induced voltages in the spinal cord and membrane polarization for an exemplary motoneuron model for electrode placement configuration LSC-S.

Figure 5. Individual EF vector components in the spinal cord for each electrode configuration as well as upward $(+)$ and downward $(-)$ electrode misplacements of $\pm 5\,\text{cm}$. Additionally, the vector component magnitude at the stimulation target is shown (right column).

$$I_{\text{syn}} = M_{\text{synapse}} * g_{\text{syn}} (V - E_{\text{R}}) \qquad (3)$$

where g_{syn} is the synaptic conductivity, V is the presynaptic voltage, E_{R} the reversal potential of the ion species involved and M_{synapse} is a gain. We model synaptic modulation by changing M_{synapse}. According to Rahman and co-workers, axon terminal hyperpolarization/depolarization leads to an increase/decrease of postsynaptic EPSP amplitude (Rahman *et al* 2013). We express the reported relationship between the EF along the axon terminal E_{axon} and synaptic conductivity gain M_{synapse} via a simple linear regression function:

$$M_{\text{synapse}} = 1 + \left(0.25/16\,(\text{V}\,\text{m})^{-1}\right) * E_{\text{synapse}}\,(\text{V}\,\text{m})^{-1} \qquad (4)$$

with 'synapse' being either an efferent or afferent synapse. All previous human tsDCS studies used placement configuration LSC-S (figure 1) which we will therefore use for further
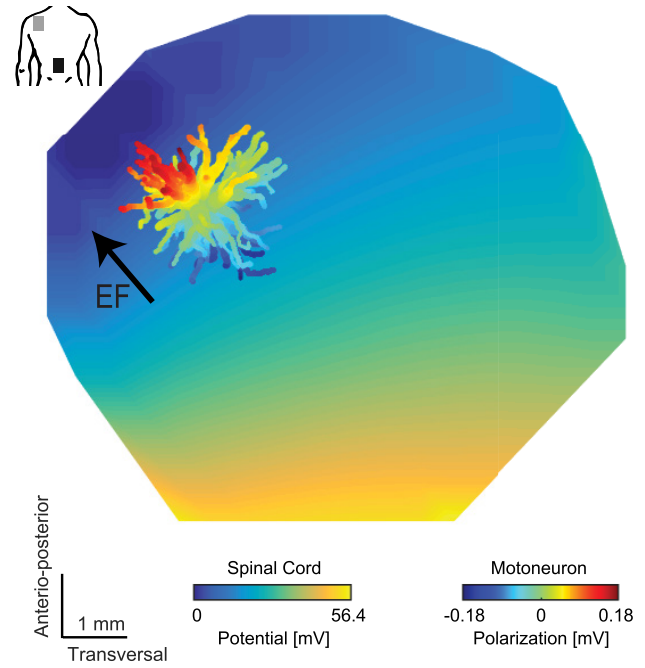
analysis. The potential distribution at motoneuron level and the direction of the resulting axon terminal polarization for configuration LSC-S in both polarities is illustrated in figure 8. Efferent and afferent axon fibers point in negative longitudinal and positive sagittal directions respectively. The EF's along both terminals are $E_{\text{efferent}} = 0.14\,\text{V}\,\text{m}^{-1}$ and $E_{\text{afferent}} = -0.24\,\text{V}\,\text{m}^{-1}$. This results in $M_{\text{efferent, acute}} = 1.002\,27$ and $M_{\text{afferent, acute}} = 0.99\,618$.

We subsequently utilize the spinal network model, to simulate the EMG responses with either efferent or afferent neural input and respectively altering $M_{\text{efferent}}/M_{\text{afferent}}$. We simulate two conditions, pulsed descending drive soleus contraction (mimicking a primary MEP response) and the H-Reflex for varying stimulation amplitudes. We perform a sensitivity analysis of the model output by increasing/decreasing the conductivity gain $M_{\text{efferent/afferent}}$ with values between 0.75 and 1.25 in increments of 0.025. To compensate for the underlying random variables in the spinal network model, the extracted variables are fit to a regression function, given their corresponding $M_{\text{efferent}}/M_{\text{afferent}}$ using the least squares method. The regression function is then utilized to estimate the modulation strength for $M_{\text{synapse, acute}}$.

The simulated MEP responses for $M_{\text{efferent}} = [0.75, 1, 1.25]$ are shown in figure 9(A). Thereby increasing synaptic gains result in higher peak amplitudes and decreasing latencies. Decreasing synaptic gains lead to the opposite effects. This is illustrated in figure 9(B), which shows both EMG amplitude and delay as a function of M_{efferent}. Signal delay and M_{efferent} followed a linear relationship, whereas the changes in amplitude were fit to an exponential of the form $a * x^b$. For $M_{\text{efferent}} = M_{\text{efferent, acute}}$ the resulting changes in amplitude and delay were 0.0163% and 0.0173 ms respectively.
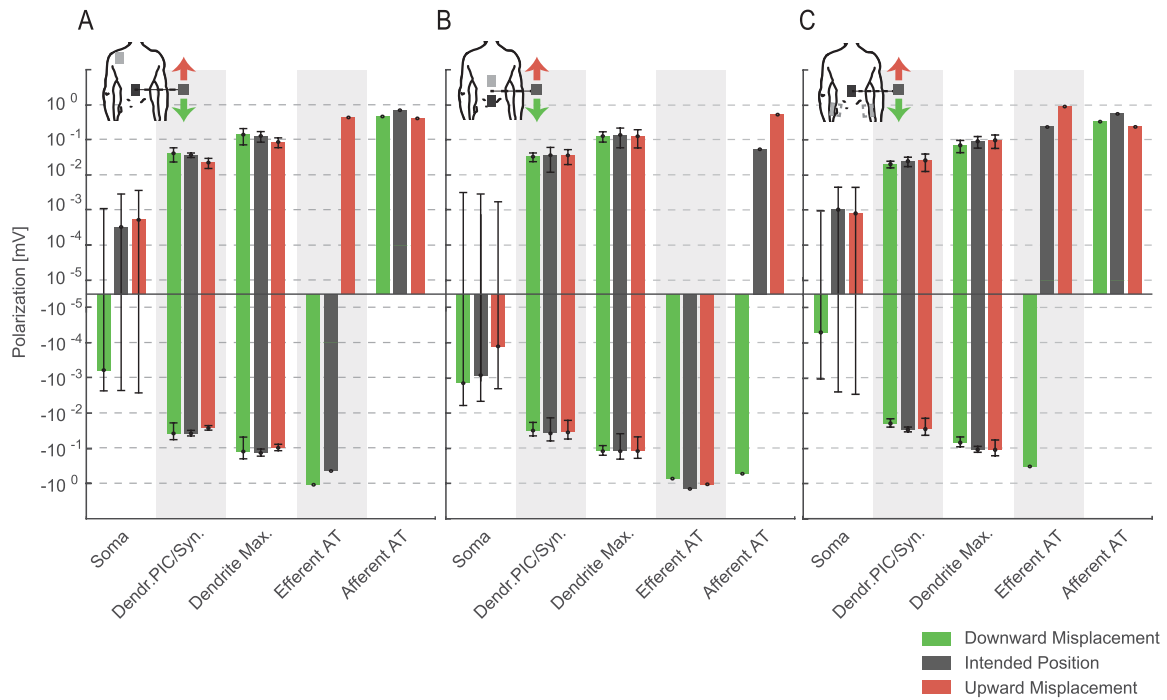
Figure 7. The average local membrane polarization and standard deviation of the six different motoneuron models. Shown are the polarization effects for: the soma, dendrites with distance to soma of less than 0.7 mm (indicating the majority of PIC channels and synaptic locations) and maximum dendritic polarization. Furthermore, polarization effects are shown for the efferent and afferent ATs respectively. The polarization is shown for the intended electrode positions as well as downward and upward 5 cm electrode position misplacements. Note that polarization intensity is drawn on a hyperlog scale (Bagwell 2005), which is linear between -10^{-5} and 10^{-5} and logarithmic otherwise.

The simulated H-reflex recruitment curves and a linear estimation of the resulting curve shift for varying $M_{afferent}$ are illustrated in figure 10. Thereby increasing/decreasing $M_{afferent}$ induces a clear left/right shift of the H-Reflex recruitment curve. This is visible in figure 10(A), which illustrates sampled recruitment curves with $M_{afferent}$ equal to 0.75, 1 and 1.25 respectively. Figure 10(B) quantifies the change. For $M_{synapse} = M_{afferent, acute}$ the resulting right shift is 0.0477%.

4. Discussion

The goal of our work was to get a better understanding of the effects generated by lumbar trans-spinal DC stimulation. This included an understanding of the EF strength, the resulting membrane polarization in spinal motoneurons and the ATs of its main incoming connections. Furthermore, we asked whether a distinct cellular target was present and the kind of acute effects this would result in. A final question was, how important a precise placement of the active electrode is at the motoneuron level and what consequences misplacement would result in.

4.1. EF distribution. We simulated the EF in the spinal cord for three different electrode configurations. For all three configurations the maximum EF amplitude inside the spinal cord, typically about midway between active and return electrode, ranged from 0.47 V m^{-1} to 0.82 V m^{-1}. This is in the same range as previously reported by Parazzini *et al* (0.6539 mV mm^{-1}) for tsDCS (Parazzini *et al* (2014)) as well as field strengths estimated for tDCS (0.15 mV mm^{-1} (Rampersad

et al 2014), 0.22 mV mm^{-1} (Miranda *et al* 2006)). From other studies it can be concluded, that the estimated EF magnitude is also sufficient to theoretically elicit lasting plasticity effects under the correct experimental conditions. Fritsch and co-workers thereby used a field strength of ~0.75 mV mm^{-1} to induce steadily increasing synaptic plasticity effects over a period of 60 min in slices from mouse primary motor cortex *in vitro* (Fritsch *et al* 2010). Furthermore, stimulation safety has to be considered. With an EF magnitude of 0.6 mV mm^{-1}, a current density of 0.01032 mA cm^{-2} is reached in the spinal white matter. Due to the differences in conductivity, values in the gray matter are ~10 times lower than that. The values obtained here are therefore more than a thousand fold lower than the safety limits for tissue damage reported in literature (Bikson *et al* 2009, Liebetanz *et al* 2009, Nitsche *et al* 2013). We further note that the EF distribution reveals a spatial pattern of cyclic in- and decrease, caused by vertebral body interference with the EF. In locations where the EF is generally small, this may lead to an additional unexpected decrease in magnitude, which might influence the intervention outcome.

4.2. Cellular target and agreement with functional morphology. We further analyzed the acute polarization effects on six realistic spinal motoneuron models. On the search for a possible cellular target, we followed the assumption that the level of local membrane polarization is directly related to the resulting functional modulation. We found that the largest polarization effects were to be expected at the ATs, with little to negligible polarization at the proximal dendrites
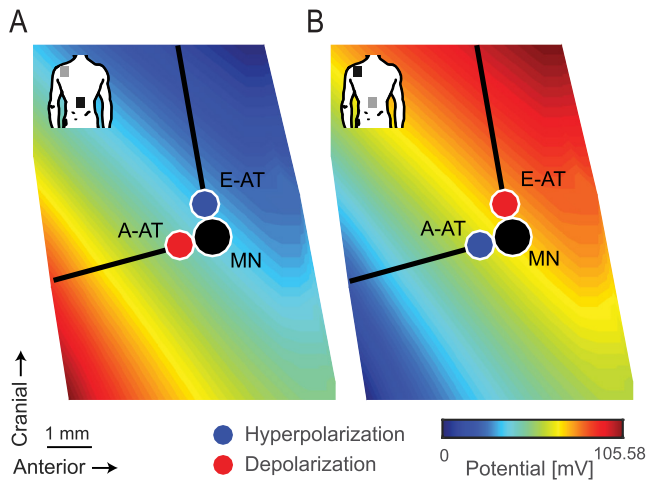
Figure 8. Simulated potential distribution in spinal cord for configuration LSC-S in both polarities as well as the estimated axon terminal polarization for efferent (E-AT) and afferent (A-AT) ATs in both cases.

Figure 9. Simulated MEP for decreasing and increasing efferent synaptic conductivity ($M = M_{efferent} = 1$, 0.75 and 1.25) (A). Individual values for MEP amplitude and delay as well as the estimated regression function for both variables, with varying $M_{efferent}$ (B).

and soma (figure 7). This is consistent over all six tested motoneuron models. We therefore conclude, that ATs are likely the most dominant cellular target in lumbar spinal DCS.

Somatic polarization is thought to be able to directly influence the generation of action potentials, which takes place close to the axon hillock. However due to the central location of the soma, with dendrites extending radially in all directions, the soma is not polarized. Therefore a direct influence on action potential generation is unlikely.

Dendrite polarization is a second source for possible functional modulation, since they are the primary location for both, incoming synaptic terminals and channels mediating PIC. However, the dendritic membrane polarization found here is low (<0.037 mV). We therefore conclude that dendritic polarization is unable to contribute to the functional modulation effects observed after tsDCS. This is supported by the lack of functional organization that seems to underlie dendritic and synaptic morphology. Nonetheless, in a modeling study Elbasiouny and Mushahwar have previously shown that the effect of an imposed EF on neural firing and PIC behavior is not directly proportional to the induced polarization. Whereas dendrite depolarization led to a decrease, hyperpolarization did not lead to a drastic change in persistent inward current (Elbasiouny and Mushahwar 2007). This implies that dendrite polarization, regardless of EF orientation, is still able to lead to a depression of motoneuron function. However, due to low dendritic membrane polarization found by us, these mechanisms will likely have a relatively small impact compared to the effects induced by axon terminal polarization.

The largest polarization effect occurred at the terminals of incoming axonal connections with maxima ranging from 0.24 mV to 1.41 mV. This is several orders of magnitude larger than the polarization values found for other neuronal structures. The correlation of direction and function for incoming axonal fibers (Burke and Glenn 1996), the dominance of axon terminal polarization (figure 7) and the lack of functional organization within synaptic/PIC channels on
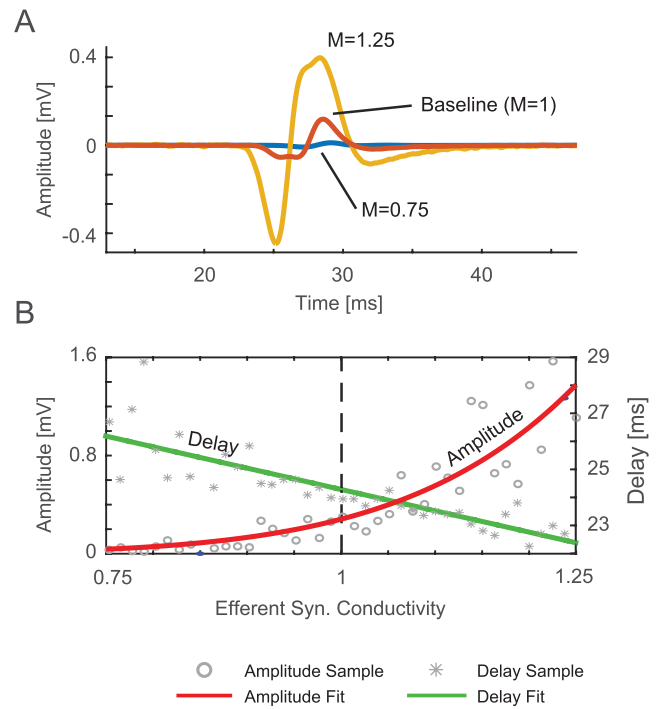
the cellular membrane therefore implicate ATs to be the most likely cellular target in lumbar spinal DCS. This conclusion is backed by previous studies which provide strong evidence that the modulatory effect caused by DC stimulation is indeed dependent on axonal orientation with respect to the applied EF (Kabakov *et al* 2012).

4.3. EF distribution and polarization for misplacements. Finding the correct vertebrae can sometimes be difficult, depending on subject anatomy. Therefore, we investigated how sensitive the EF distribution is to electrode misplacements. The results suggest that a longitudinal offset of 5 cm (ca. 1.5 vertebrae lengths) is sufficient to substantially alter EF magnitude direction and amplitude at the intended stimulation site. This is evident from figures 5 and 7, showing that an upward/downward electrode misplacement may even reverse axon terminal polarization. When considering the curvature of the EF, misplacements especially in cases where the stimulation site is close to the electrode may therefore have a large effect on axon terminal polarization due to the resulting change in EF direction. Therefore, electrode misplacement may be an important source of the variability experimentally observed in response to tsDCS.

4.4. From cellular to network effects. Several studies have previously investigated the effects of tsDCS on neural function. To bridge theoretical data on a cellular level, to experimental data on a functional level is challenging. We therefore included an intermediate step, comprising of a lumbar spinal
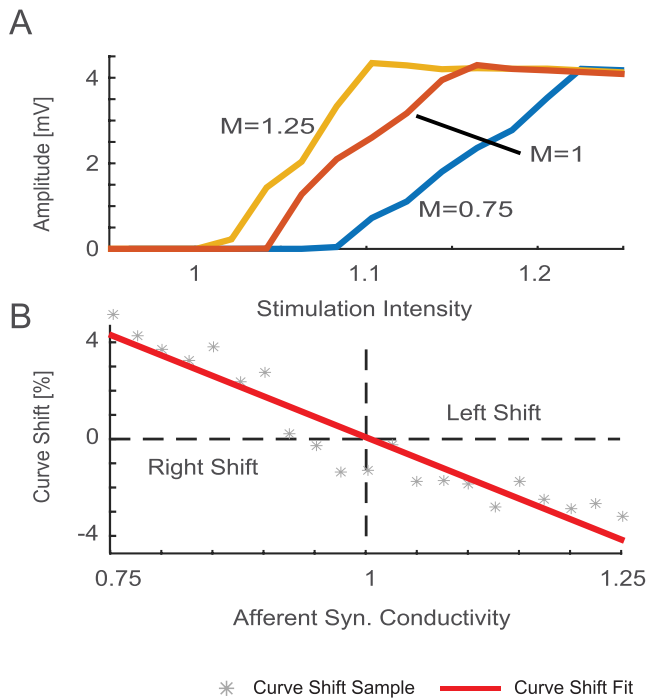
Figure 10. Simulated H-Reflex recruitment curve for varying afferent synaptic conductivity gains ($M = M_{\text{afferent}}$) (A), and the left/right shift induced by varying M_{afferent} expressed as a percentage of stimulation intensity (B).

network model (Cisi and Kohn 2008). The characteristic effects obtained for both, simulated MEP and H-Reflex responses are in accordance with what has been shown in previous studies (Lamy *et al* 2012, Hubli *et al* 2013, Bocci *et al* 2014). While changing efferent synaptic conductivity results in a modulation of the simulated MEP amplitude and latency, altering afferent synaptic conductivity leads to a well-defined left/right shift of the H-Reflex recruitment curve (figure 10). However the estimated acute changes in amplitude for both scenarios are much smaller than the long-term changes induced by tsDCS as reported in literature.

4.5. Comparison between simulated acute and reported long term effects. So far, we showed that ATs may be the likely main cellular target for tsDCS. The acute synaptic effects of axon terminal polarization are known from literature (Hubbard and Willis 1962, 1968, Rahman *et al* 2013). Additionally, we showed that synaptic conductivity changes on a network level, result in the same type of functional effects as the long term effects reported by several previous tsDCS studies. It is therefore of special interest, how axon terminal polarization—in connection with its theoretical acute synaptic conductivity effect and the simulated spinal network responses—can be connected to the effects reported experimentally by others. In the following, we therefore individually compare the experimental results obtained by others to the simulations reported here.

Anodal tsDCS can result in a significant left shift of the H-Reflex recruitment curve (Lamy *et al* 2012, Hubli *et al* 2013). Cathodal stimulation had no significant effect. For anodal tsDCS, afferent ATs are depolarized (figure 8(A)),

acutely decreasing synaptic conductivity. However network simulations imply an increasing afferent synaptic gain to replicate the effect observed experimentally (H-Reflex left shift). Acute synaptic terminal and long-term plasticity effects are therefore in opposite directions. Bocci *et al* showed an increase/decrease in motor evoked potential area for cathodal/anodal tsDCS. Modulation of MEP area can theoretically be achieved by altering motoneuron recruitment (Bocci *et al* 2014). The efferent axon terminal is depolarized/hyperpolarized for cathodal/anodal stimulation (figure 8), leading to a theoretical increase/decrease of synaptic conductivity. Network simulation indicates a larger motoneuron response for increased synaptic conductivity and vice versa. Therefore the simulated acute synaptic changes for both polarities are in opposite direction to the experimental results reported by Bocci *et al* and Winkler *et al* found an increase/decrease of PAD of the H-Reflex after cathodal and anodal tsDCS respectively (Winkler *et al* 2010). PAD, is a reduction of synaptic efficacy due to decreased neurotransmitter release at a previous activated Ia fiber-motoneuron synapse (Grey *et al* 2008) and has not been shown to be susceptible to supraspinal influences (Winkler *et al* 2010). For anodal/cathodal tsDCS the afferent axon terminal is depolarized/hyperpolarized, leading to an acute suppression/strengthening of afferent synaptic conductivity. Thus the reported experimental effects are again opposite to the acute synaptic effects estimated here. Yamaguchi *et al* showed a decrease in presynaptic inhibition of Ia afferents (D1 inhibition) for anodal tsDCS. Since D1 inhibition is mediated by descending pathways via inhibitory presynaptic connections (Rudomin 2009), effects on the efferent pathway have to be considered. For anodal tsDCS, the efferent axon terminal is hyperpolarized, leading to an acute synaptic facilitation. This stands in contrast to the depression effects reported in literature.

For all of the discussed human studies, we therefore note a long-term plasticity effect in opposite direction to the acute synaptic changes estimated here. A reversal of acute and after effect has previously been observed by others. For instance, a study by Ahmed (2011) showed a suppression, during and potentiation, after DCS of cortically evoked potentials for anodal tsDCS in mice. Switching polarities reversed the effect. Inversion of effects during versus after DCS is therefore possible. Nonetheless, the underlying mechanisms connecting acute and longer term plasticity effects remain elusive and need to be well understood for rational applications of DCS in clinical practice.

4.6. Practical implications on intervention design. We estimated the EF strength at MN level for several configurations. The EFs appeared similar to those reported in previous studies *in vitro* (Fritsch *et al* 2010), which showed significant modulatory effects on a cellular level. Thus, for any of the simulated electrode placements the EF is theoretically large enough for functional modulation, given the appropriate neural target structure and neural activity. However accurately estimating the applied EF as we did, is vital since EF direction and amplitude are equally important and intervention designs solely based on EF magnitude may potentially lead to suboptimal

results in application. This is especially evident when considering the effects of electrode misplacements on axon terminal polarization (figure 7). Thereby, misplacement of 5 cm may lead to a change in EF direction and thus result in a reversal of AT polarization. This implies that interventions should be designed such that for small misplacements, influence on EF vector angle is kept minimal, which can be achieved by either focusing on proper electrode placement or actively misplacing the electrode in a direction for which misplacement in the opposite direction would not lead to reversal of EF direction at the intended stimulation target. Additionally, vertebral bodies may lead to fluctuations of EF magnitude. This could further be taken into account by placing the electrodes such that EF fluctuations are small with respect to the overall EF amplitude.

We identified ATs to be the most dominant cellular target. It may therefore be possible to modulate individual functional pathways, under the condition that both pathways are oriented in a specific, no-random direction at different angles towards each other, optimally approaching 90°. This may to some degree be applicable to the descending and sensory fibers in the lumbar spinal cord such that pathway specific modulation may be feasible.

4.7. Limitations. We use a realistic full body, segmented, MRI model for computation of the EF after tsDCS stimulation. However, though being a realistic anatomical representation, the model is subject specific. Thus, the results presented here are not quantitatively generalizable across subjects. Nonetheless, we expect that generalization over subjects is principally possible once knowing the individualized anatomical details.

We used realistic reconstructions of motoneurons originally obtained from cats, which may limit generalization to human subjects. However, although quantitative differences may occur we believe the models nonetheless provide a reasonable basis for the intended logical reasoning. Furthermore, we represent incoming ATs with a straight cylindrical compartmental model. We expect this approximation to hold for the average of all incoming ATs. However, in a realistic scenario incoming axons branch out, forming a tree-like structure of ATs to form connections with local dendrites. Therefore axon terminal polarization will likely be distributed within a range centered around the values similar to those estimated here.

5. Conclusion

We show that the tsDCS induced EF strengths at spinal motoneuron level is similar to those that have been described for tDCS in the cortex. Furthermore, similar EF amplitudes have previously been used *in vivo* and *vitro* to evoke significant modulation in the underlying neural structures. We therefore conclude that the tsDCS generated EF in the spinal cord is of sufficient strength to evoke functional modulation. Also, axon terminal polarization is expected to be the primary cellular target, inducing the modulatory effects observed after lumbar tsDCS. However, the expected acute synaptic efficacy changes are in opposite direction to the long-term plasticity effects reported in literature. This emphasizes the need for a deeper understanding of the mechanisms involved in the transition

from acute to long-term plasticity effects. Furthermore, we show that correct electrode placement is crucial for the success of the application. Possible pitfalls such as incorrect EF alignment due to electrode misplacement should be taken into consideration in the design of electrotherapeutic interventions. This may lead to better methods for predicting the outcome of tsDCS.

Acknowledgments

References

Ahmed Z 2011 Trans-spinal direct current stimulation modulates motor cortex-induced muscle contraction in mice *J. Appl. Physiol.* **110** 1414–24

Ahmed Z 2013a Effects of cathodal trans-spinal direct current stimulation on mouse spinal network and complex multijoint movements *J. Neurosci.* **33** 14949–57

Ahmed Z 2013b Electrophysiological characterization of spino-sciatic and cortico-sciatic associative plasticity: modulation by trans-spinal direct current and effects on recovery after spinal cord injury in mice *J. Neurosci.* **33** 4935–46

Alam M *et al* 2017 Electrical neuromodulation of the cervical spinal cord facilitates forelimb skilled function recovery in spinal cord injured rats *Exp. Neurol.* **291** 141–50

Alvarez F J *et al* 1998 Distribution of 5-hydroxytryptamine-immunoreactive boutons on alpha-motoneurons in the lumbar spinal cord of adult cats *J. Comp. Neurol.* **393** 69–83

Arlotti M *et al* 2012 Axon terminal polarization induced by weak uniform DC electric fields: a modeling study *2012 Annual Int. Conf. of the IEEE Engineering in Medicine and Biology Society* vol 2012 pp 4575–8

Bagwell C B 2005 HyperLog—a flexible log-like transform for negative, zero, and positive valued data *Cytometry* A **64** 34–42

Balbi P, Martinoia S and Massobrio P 2015 Axon-somatic back-propagation in detailed models of spinal alpha motoneurons *Front. Comput. Neurosci.* **9** 15

Bikson M *et al* 2004 Effects of uniform extracellular DC electric fields on excitability in rat hippocampal slices *in vitro J. Physiol.* **557** 175–90

Bikson M, Datta A and Elwassif M 2009 Establishing safety limits for transcranial direct current stimulation *Clin. Neurophysiol.* **120** 1033–34

Bikson M, Name A and Rahman A 2013 Origins of specificity during tDCS: anatomical, activity-selective, and input-bias mechanisms *Front. Human Neurosci.* **7** 688

Bindman L J, Lippold O C and Redfearn J W 1964 The action of brief polarizing currents on the cerebral cortex of the rat (1) during current flow and (2) in the production of long-lasting after-effects *J. Physiol.* **172** 369–82

Bocci T *et al* 2014 Cathodal transcutaneous spinal direct current stimulation (tsDCS) improves motor unit recruitment in healthy subjects *Neurosci. Lett.* **578** 75–9

Boron W F and Boulpaep E L 2012 *Medical Physiology* (Philadelphia, PA: Elsevier)

Burke B R E 1968 Group Ia synaptic input to fast and slow twitch motor units of cat triceps surae *J. Physiol.* **196** 605–30

Burke R E and Glenn L L 1996 Horseradish peroxidase study of the spatial and electrotonic distribution of group Ia synapses on type-identified ankle extensor motoneurons in the cat *J. Comp. Neurol.* **372** 465–85

Carnevale N T and Hines M L 2009 *The NEURON Book* (New York: Cambridge University Press)

Christ A *et al* 2010 The virtual family—development of surface-based anatomical models of two adults and two children for dosimetric simulations *Phys. Med. Biol.* **55** N23–38

Cisi R R L and Kohn A F 2008 Simulation system of spinal cord motor nuclei and associated nerves and muscles, in a Web-based architecture *J. Comput. Neurosci.* **25** 520–42

Cogiamanian F *et al* 2008 Effect of spinal transcutaneous direct current stimulation on somatosensory evoked potentials in humans *Clin. Neurophysiol.* **119** 2636–40

Cogiamanian F *et al* 2012 Transcutaneous spinal direct current stimulation *Front. Psychiatry* **3** 63

Datta A *et al* 2009 Gyri-precise head model of transcranial direct current stimulation: improved spatial focality using a ring electrode versus conventional rectangular pad *Brain Stimul.* **2**

Di Lazzaro V *et al* 2003 Corticospinal volleys evoked by transcranial stimulation of the brain in conscious humans *Neurol. Res.* **25** 143–50

Elbasiouny S M and Mushahwar V K 2007 Suppressing the excitability of spinal motoneurons by extracellularly applied electrical fields: insights from computer simulations *J. Appl. Physiol.* **103** 1824–36

Fritsch B *et al* 2010 Direct current stimulation promotes BDNF-dependent synaptic plasticity: potential implications for motor learning *Neuron* **66** 198–204

Gartside I B 1968 Mechanisms of sustained increases of firing rate of neurons in the rat cerebral cortex after polarization: reverberating circuits or modification of synaptic conductance? *Nature* **220** 382–3

Grey M J *et al* 2008 Post-activation depression of Soleus stretch reflexes in healthy and spastic humans *Exp. Brain Res.* **185** 189–97

Hall J E and Guyton A C 2006 *Textbook of Medical Physiology* (Philadelphia, PA: Elsevier)

Harkema S *et al* 2011 Effect of epidural stimulation of the lumbosacral spinal cord on voluntary movement, standing, and assisted stepping after motor complete paraplegia: a case study *Lancet* **377** 1938–47

Heckman C J *et al* 2008 Persistent inward currents in spinal motoneurons and their influence on human motoneuron firing patterns *Neuroscientist* **14** 264–75

Hubbard J I and Willis W D 1962 Hyperpolarization of mammalian motor nerve terminals *J. Physiol.* **163** 115–37

Hubbard J I and Willis W D 1968 The effects of depolarization of motor nerve terminals upon the release of transmitter by nerve impulses *J. Physiol.* **194** 381–405

Hubli M *et al* 2013 Modulation of spinal neuronal excitability by spinal direct currents and locomotion after spinal cord injury *Clin. Neurophysiol.* **124** 1187–95

Jefferys J G 1981 Influence of electric fields on the excitability of granule cells in guinea-pig hippocampal slices *J. Physiol.* **319** 143–52

Kabakov A Y *et al* 2012 Contribution of axonal orientation to pathway-dependent modulation of excitatory transmission by direct current stimulation in isolated rat hippocampus *J. Neurophysiol.* **107** 1881–89

Lamy J-C and Boakye M 2013 BDNF Val66Met polymorphism alters spinal DC stimulation-induced plasticity in humans *J. Neurophysiol.* **110** 109–16

Lamy J-C *et al* 2012 Modulation of soleus H reflex by spinal DC stimulation in humans *J. Neurophysiol.* **108** 906–14

Liebetanz D *et al* 2009 Safety limits of cathodal transcranial direct current stimulation in rats *Clin. Neurophysiol.* **120** 1161–7

Midroni G and Bilbao J M 1995 *Chapter 3—Quantitative Techniques BT—Biopsy Diagnosis of Peripheral Neuropathy* (Portsmouth, NH: Heinemann) pp 35–43

Miranda P C 2013 Physics of effects of transcranial brain stimulation *Brain Stimulation. Handbook of Clinical Neurology* ed A M Lozano and M Hallett (Amsterdam: Elsevier) ch 29, pp 353–66

Miranda P C, Lomarev M and Hallett M 2006 Modeling the current distribution during transcranial direct current stimulation *Clin. Neurophysiol.* **117** 1623–9

Nitsche M A *et al* 2013 Safety criteria for transcranial direct current stimulation (tDCS) in humans *Clin. Neurophysiol.* **133** 285

Parazzini M, Fiocchi S, Liorni I, Rossi E, Cogiamanian F, Vergari M, Priori A and Ravazzani P 2014 Modeling the current density generated by transcutaneous spinal direct current stimulation (tsDCS) *Clin. Neurophysiol.* **125** 2260–70

Patestas M and Gartner L P 2006 *A Textbook of Neuroanatomy* (Hoboken, NJ: Wiley)

Powers R K *et al* 2012 Contribution of intrinsic properties and synaptic inputs to motoneuron discharge patterns: a simulation study *J. Neurophysiol.* **107** 808–23

Radman T *et al* 2009 Role of cortical cell type and morphology in subthreshold and suprathreshold uniform electric field stimulation in vitro *Brain Stimul.* **2** 215–228.e3

Rahman A *et al* 2013 Cellular effects of acute direct current stimulation: somatic and synaptic terminal effects *J. Physiol.* **591** 2563–78

Rampersad S M *et al* 2014 Simulating transcranial direct current stimulation with a detailed anisotropic human head model *IEEE Trans. Neural Syst. Rehabil. Eng.* **22** 441–52

Ranieri F *et al* 2012 Modulation of LTP at rat hippocampal CA3-CA1 synapses by direct current stimulation *J. Neurophysiol.* **107** 1868–80

Rotterman T M *et al* 2014 Normal distribution of VGLUT1 synapses on spinal motoneuron dendrites and their reorganization after nerve injury *J. Neurosci.* **34** 3475–92

Rudomin P 2009 In search of lost presynaptic inhibition *Exp. Brain Res.* **196** 139–51

Salvador R *et al* 2010 Modeling the electric field induced in a high resolution realistic head model during transcranial current stimulation *2010 Annual Int. Conf. of the IEEE Engineering in Medicine and Biology Society* pp 2073–6

Segev I, Fleshman J W and Burke R E 1990 Computer simulation of group Ia EPSPs using morphologically realistic models of cat alpha-motoneurons *J. Neurophysiol.* **64** 648–60

Wenger N *et al* 2016 Spatiotemporal neuromodulation therapies engaging muscle synergies improve motor control after spinal cord injury *Nat. Med.* **22** 138–45

Winkler T, Hering P and Straube A 2010 Spinal DC stimulation in humans modulates post-activation depression of the H-reflex depending on current polarity *Clin. Neurophysiol.* **121** 957–61

Yamaguchi T *et al* 2013 Effects of transcutaneous spinal DC stimulation on plasticity of the spinal circuits and corticospinal tracts in humans *2013 6th Int. IEEE/EMBS Conf. on Neural Engineering (NER)* pp 275–8